Impact of cell wall non-cellulosic and cellulosic polymers on the mechanical properties of flax fibre bundles

Maxime Gautreau, Sylvie Durand, Angeline Paturel, Sophie Le Gall, Loïc Foucat, Xavier Falourd, Bruno Novales, Marie-Christine Ralet, Sylvie Chevallier, Antoine Kervoelen, et al.

Version of Record: https://www.sciencedirect.com/science/article/pii/S0144861722005045
Manuscript_d7737058b5ddf3d0d488510559239213

Impact of cell wall non-cellulosic and cellulosic polymers on the mechanical properties of flax fibre bundles

Maxime Gautreau[1], Sylvie Durand[1], Angeline Paturel[1,2], Sophie Le Gall[1,4], Loic Foucat[1,4], Xavier Falourd[1,4], Bruno Novales[1,4], Marie-Christine Ralet[1], Sylvie Chevallier[5], Antoine Kervoelen[3], Alain Bourmaud[3], Fabienne Guillon[1] and Johnny Beaugrand[1]*

[1] : INRAE, UR BIA, F-44316 Nantes,

[2] : Université de Lille, UMR-CNRS 8207, UMET, F-59652 Villeneuve d'Ascq, France

[3] : Univ. Bretagne Sud, UMR CNRS 6027, IRDL, F-56100 Lorient, France

[4] : INRAE, BIBS facility, PROBE infrastructure, F-44316 Nantes, France

[5] : Oniris, Nantes Université, CNRS, GEPEA, UMR 6144, F-44000 Nantes, France

* Corresponding author: johnny.beaugrand@inrae.fr

Abstract

Fibre bundles are groups of elementary fibres glued together thanks to the middle lamella, and are the main fraction in plant fibre composites. In this study, relationship between the mechanical properties of flax fibre bundles, chemical composition and cellulose structure were investigated. To do so, a sequential biopolymer extraction was implemented. Fibre bundles were first depectinated by oxalate extraction, and then the hemicelluloses were extracted by LiCl/dimethyl sulfoxide (DMSO) and KOH. The oxalate extract consisted of homogalacturonans and type I rhamnogalacturonans, while the LiCl extract was composed mainly of glucomannans and the KOH extract of xyloglucans. The KOH stage resulted in the appearance of cellulose II in flax bundles. The extraction of pectin and hemicelluloses led to the disappearance of the middle lamella concomitant with a decrease in the tensile Young's modulus and maximum strength. Finally, the fibre bundle composition, ultrastructure and mechanical properties are discussed together in view of the thin middle lamella.

Keywords

Flax – Fibre bundles - Mechanical properties – Sequential extraction – Polysaccharides

1 Introduction

Plant fibres offer several advantages to reduce the environmental impacts of human activities. Among them, flax fibres coming from renewable resources have a low density (Fu, Lauke, Mäder, Yue, & Hu, 2000) and specific mechanical properties equivalent to glass fibres (Lefeuvre, Bourmaud, Morvan, & Baley, 2014), which are among the best plant fibres (Bourmaud, Shah, Beaugrand, & Dhakal, 2020).

Within the stem, the flax fibres are located in the phloem area and are present as bundles of several tens of single fibres (Akin, Gamble, Morrison, Rigsby, & Dodd, 1996). Fibres are individual cells characterized by an elongated polygonal shape, a reduced lumen volume and a thick cell wall. Their length can reach several centimetres with a diameter between ten and twenty microns (Pillin et al., 2011). At maturity, the plant cell wall of flax fibre consists, from the outside towards the inside, of the primary cell wall, secondary cell wall. Finally, in the middle of the fibre is a central cavity called the lumen (T. Gorshkova & C. Morvan, 2006), which can be irregular (E. Richely et al., 2021). The pectin-rich middle lamella ensures cohesion between fibres (Lazic, Janjic, Rijavec, & Kostic, 2017), but this thin layer is also considered as a weakness point that flax producers try to degrade and eliminate through retting, scutching and combing stages to provide composite reinforcements as individualised as possible. The soft primary wall is rather intricate with the middle lamella (Melelli, Arnould, Beaugrand, & Bourmaud, 2020) and has a thickness of approximately 0.2 µm (T. A. Gorshkova et al., 1996). The soft primary wall consists of a matrix composed of hemicelluloses and pectins, which embeds randomly oriented cellulose microfibrils (Nilsson & Gustafsson, 2007), even if recent studies tend to show an orientation in the axis of the fibre (Baley, Goudenhooft, Gibaud, & Bourmaud, 2018). The secondary wall is much thicker, the thickness of classical secondary wall usually is 2-4 µm with an S1 sublayer typically in the range of 0.1-0.4 µm. In the case of bast fibers, thickness of up to 10 µm can be reached due to the presence of a gelatinous layer. At maturity, the G layer is the main layer of the flax fibres (Bourmaud, Beaugrand, Shah, Placet, & Baley, 2018; T. Gorshkova, Chernova, Mokshina, Ageeva, & Mikshina, 2018). It is composed mainly of highly crystalline cellulose (Bos, 2004) and pectic type I rhamnogalacturonan (RGI) decorated with ß (1-4) galactan side chains (3-7%) (Tatyana Gorshkova & Claudine Morvan, 2006) and, to a lesser extent, arabinogalactan protein and glucomannan (T.

Gorshkova, Chernova, Mokshina, Gorshkov, et al., 2018) (T. A. Gorshkova et al., 2010; C. Morvan et al., 2003). Xylan and lignin are absent in the G layer but xyloglucan has been detected in flax phloem fiber (Claudine Morvan et al., 2003). A possible role of xyloglucan in the binding of S- and G-layers have even been proposed (T. Gorshkova et al., 2015).

RGI are thought to play a major role in the formation and properties of the G layer. They undergo modification in the developing fibre (Tatyana Gorshkova & Claudine Morvan, 2006) (Gurjanov, Ibragimova, Gnezdilov, & Gorshkova, 2008). During the deposition of the gelatinous cell walls, RGI with long galactan chains is formed. The long galactan chains can serve as spacer between cellulose microfibrils, preventing their lateral interactions. As the fibre mature, the galactan side chains are trimmed off by galactosidase allowing lateral interactions between cellulose microfibrils that lead to RGI entrapment (T. Gorshkova, Chernova, Mokshina, Ageeva, et al., 2018) and specific mechanical properties of the G layer (Olivier Arnould, David Siniscalco, Alain Bourmaud, Antoine Le Duigou, & Christophe Baley, 2017).

If many studies have examined the mechanical properties of the secondary wall sublayers (O. Arnould, D. Siniscalco, A. Bourmaud, A. Le Duigou, & C. Baley, 2017), few studies are available regarding the weakness points that glue strong individual fibres together. For instance, the reported interfacial shear stress in flax is only 2.9 MPa between two fibres (Charlet & Beakou, 2011). Morphologically speaking, a fibre bundle is a composite structure made of individual fibres and an interface bonding layer, the compounded middle lamella. Therefore, fibre bundle mechanical properties also depend on the middle lamella and the primary cell wall and on their composition. Due to the low investigation scale required, only local, but non absolute, investigation techniques, such as atomic force microscopy in Peakforce mode (AFM-PF) can be used to estimate the indentation modulus of the middle lamella; a value of 10.2 ± 1.2 GPa was reported (Melelli et al., 2020), compared to an indentation value of 18.0 ± 1.9 GPa for a flax G layer (Goudenhooft et al., 2018).

Middle lamellae are enriched in non-cellulosic polymers, and mechanically speaking, hemicelluloses and pectins have been demonstrated to have a specific function as cell wall plasticizers, enabling the individual fibre to reach interesting values of strain and stress during mechanical loading (Lefeuvre et al., 2015) (Gourier, Le Duigou, Bourmaud, & Baley, 2014).

In flax, indirect investigations of the relationship between biochemical composition and mechanical properties were long ago investigated by affinity solvent extraction strategy (Lindeberg, 1948). Pectins were generally extracted sequentially by boiling water and by a chelating agent, usually ethylene diaminetetraacetic acid (EDTA) (Goubet et al., 1995). Then, a strong acid is often used (HCl or H_2SO_4), followed by a soda extraction (NaOH or KOH) aiming to extract the polysaccharides strongly linked in the cell wall, mostly hemicelluloses and structural pectins (Alix, Goimard, Morvan, & Baley, 2009) (Lefeuvre, Bourmaud, Lebrun, Morvan, & Baley, 2013). At the scale of elementary fibres, both Young's modulus and the tensile strength at break have been shown to decrease almost linearly with the extraction stages, while the strain at rupture remains almost constant (Lefeuvre et al., 2015). In particular, acid-extracted polysaccharides, so-called matrix noncellulosic polysaccharides (NCPs), were shown to influence the strength, while alkali-extracted polysaccharides, so-called structuring NCPs, have mainly an effect on the stiffness. At the scale of the fibre bundles, such data are not available.

In the same way, no data exist on the changes induced by both extraction and immersion in solvent at the ultrastructural level and how these changes influence the mechanical properties. Indeed, the alteration of the polymer linkages and arrangements can lead to changes in the properties of fibre elements. Solid-state nuclear magnetic resonance (ssNMR) has been validated as a method of choice to probe ultrastructural features in plant cell walls. The ssNMR has been used to monitor flax cell wall evolution during retting (Bourmaud, Siniscalco, et al., 2018).

The ambitious aim of this research work is to fill a gap in the knowledge of the relationships between the biochemical composition of bundles, polymer ultrastructure and mechanical properties on the scale of flax fibre bundles, including the middle lamella. To do so, sequential extraction was performed, and fine chemical analysis was carried out on the extracted components, including glycosidic linkage analysis of cell wall polysaccharides by direct and indirect methods. Parallel, the ultrastructural modifications generated by the extraction stages were characterized by NMR approaches, solid-state CP-MAS (cross polarization-magic angle spinning) in residual treated bundles and low field relaxometry. Finally, the fibre bundle tensile properties and the results of multiscale biochemical analysis are discussed and compared to the literature data and statements dealing with individual fibres. Definitely, the main

ambition of the present work is to address precise elements on the contribution of the middle lamella and its constitutive polymers in the mechanical properties of bundles; these findings would be of great interest for better understand the damage mechanism and mechanical behaviour of bundles during the manufacturing or used of biobased composite materials.

2 Materials and methods

2.1 Materials

The scutched flax fibres (Avian variety, 2017) were provided by the Van Robaeys Frères Company (Killem, 59, France). They were sown in March, pulled out at the end of June and then dew-retted in the field for 6 weeks. Then, they were mechanically extracted on an industrial scutching line.

2.2 Sequential solvent extractions

The sequential extraction stages are summarized in Figure 2 and correspond to the protocol described by Lefeuvre et al. (Lefeuvre et al., 2015) and slightly modified according to Assor et al. (Assor, Quemener, Vigouroux, & Lahaye, 2013).

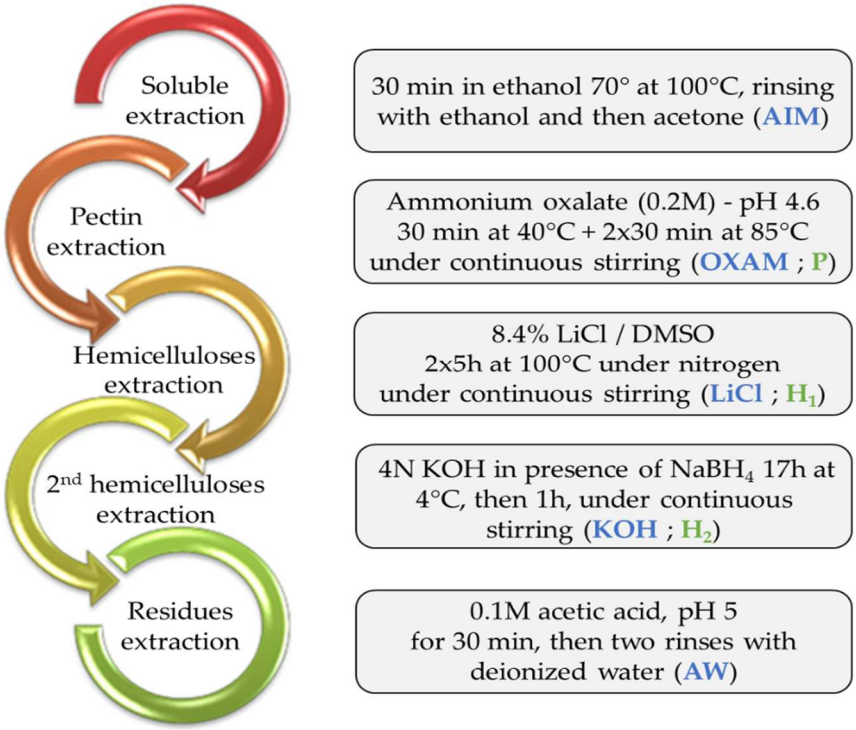

Figure 1. Scheme of the sequential polysaccharide extractions and of the extracted products. (AIM= Alcohol Insoluble Material; OXAM = oxalate extraction and corresponding extract P enriched in pectins, LiCl= lithium chloride extraction and corresponding extract H1 enriched in easily extractable

hemicelluloses; KOH= potassium hydroxide and corresponding extract H2 enriched in strongly linked hemicelluloses; AW = acidified water)

Indeed, a supplementary extraction stage with LiCl and dimethyl sulfoxide (DMSO) was incorporated to selectively extract weakly bonded hemicelluloses. Alcohol-insoluble material (AIM) was obtained after boiling fibres for 20 min in 70% ethanol (15 g/250 mL). AIM was transferred to a G2 sintered glass filter, and the alcohol was removed by aspiration under vacuum. AIM was washed several times with 70% ethanol and then twice with absolute ethanol for 30 min. Finally, AIM was dried with acetone and weighed to determine the yield.

For pectin extraction, AIM (~15 g dry weight) was suspended in 300 mL of 0.2 M ammonium oxalate solution at pH 4.6. Extraction of pectin was carried out at 40 °C for 30 min and then at 85 °C for 30 min under stirring. Solid/liquid separation was carried out by filtering under vacuum onto G3 sintered glass. The extraction at 85 °C for 30 min was repeated twice. Each time, the liquid fraction was recovered. Then, the residual AIM was washed twice with 200 mL of deionized water. The three extracts and the washings were pooled, concentrated and dialyzed (MWCO 6000-8000) against deionized water until the conductivity of the washes reached 3 µS/cm. Finally, the pectin-enriched extract (**P**) was freeze-dried.

Hemicellulose extraction was carried out according to Ray et al. (2014) (Ray, Vigouroux, Quemener, Bonnin, & Lahaye, 2014). The oxalate-treated bundles were suspended in 8.4% (w/v) LiCl/DMSO (14.56 g dry weight for 500 mL) at 100 °C for 5 h under agitation and N_2. Then, the sample was centrifuged at 30,000 *g* for 15 min. The process was repeated twice. After each centrifugation, the supernatants were recovered, centrifuged at 30,000 *g* for 30 min and filtered on G3 sintered glass. The treated bundles were washed with DMSO for 15 min. The washing operation was repeated until the residual fibres were clean. The LiCl/DMSO extracts and DMSO washings were pooled and evaporated to dryness at 60 °C under vacuum. The LiCl/DMSO extract was dissolved in deionized water, precipitated with 4 volumes of absolute ethanol at 4 °C, and left to decant overnight at 4 °C. The precipitate was recovered by centrifugation (12 min at 30,000 *g*), washed with absolute ethanol and finally dried at 40 °C under vacuum. This extract corresponding to the first population of hemicelluloses was named **H1**.

The LiCl/DMSO-treated bundles (13.82 g) were extracted with 4 M KOH (600 mL) for 17 h at room temperature under stirring and in the presence of $NaBH_4$ (0.03 g/L). The suspension was centrifuged (32,000 *g*, 23 min), and the supernatant was filtered on G3 sintered glass. This stage was repeated with an incubation time of 1 hour. The pellet was recovered and washed with 0.1 M acetic acid and deionized water until the washing water was no longer alkaline. The final solid-treated bundles were dried at 40 °C under vacuum. The KOH extracts were neutralized with acetic acid, dialyzed (MWCO 6000-8000) against osmosis water until the conductivity of washes reached 3 µS/cm. The neutralized KOH extracts were concentrated approximately 3 times and freeze-dried. This extract corresponding to the second family of more strongly linked hemicelluloses was named **H2**.

Finally, the KOH-treated bundles (13.54 g) were subjected to a final extraction with acidified water (AW, 1 L) for 20 min under stirring. The suspension was centrifuged (32 000 *g*, 15 min). The pellet was transferred to GX sintered glass and washed with deionized water until the pH was neutral. The treated bundles were dried at 40 °C under vacuum. The extract was neutralized with NH_3, dialyzed (MWCO 6000-8000) and freeze-dried.

2.3 Characterizations

2.3.1 Tensile properties of flax bundles

The tensile tests were carried out on an MTS Criterion Series 40 (MTS, Eden Prairie, Minnesota, USA) equipped with a 5 N force cell. The diameter of each bundle was measured at 6 different locations using a Nikon macroscope (Nikon, Tokyo, Japan) (Lefeuvre et al., 2014). The diameters of the bundles tested ranged between 75 and 125 µm for the different stages of sequential extraction. The bundles were glued in a cardboard frame having a nominal length of 70 mm according to Charlet et al. (Charlet & Beakou, 2011). The frame was then placed in the jaws of the traction machine. Then, the edges of the paper frame were cut so that traction was only carried out on the bundle. The displacement speed was 1 mm/min, and data were recorded with a frequency of 100 Hz. The results shown are an average of at least 30 validated tensile tests. Tensile tests were performed at 23 °C and 50% relative humidity in a controlled environment.

2.3.2 Surface analysis of flax fibres

Scanning electron microscopy (SEM) observations were performed on a field emission gun scanning electron microscope (Thermo Fischer Scientific, Quattro S, Waltham, Massachusetts, USA). Images were recorded at an acceleration voltage of 6 kV and a pressure of 80 Pa using the LV detector. Five fibre bundles by modality were cut and glued to a carbon pellet placed on the sample holder. The samples have not been metallized.

2.3.3 Biochemical composition of flax fibres

2.3.3.1 Mid-infrared spectroscopy

Treated bundles and extracts were analysed by mid-infrared spectroscopy (IR) with a Thermo Nicolet IS50 spectrometer (ThermoFisher Scientific, Courtaboeuf, France), as shown in Figure 4. Two milligrams of ground sample was mixed with 120 mg of potassium bromide (KBr) and pressed to obtain a KBr pellet. One pellet without sample was prepared to make the blank. Spectra were collected in transmission mode in the 4000-600 cm^{-1} infrared range at a resolution of 16 cm^{-1} with 200 added scans using OMNIC software (V 9.2.41). All spectra were preprocessed using OPUS 7.5 (Bruker Optics). The spectra in the 2000 and 700 cm^{-1} regions were smoothed at five points, corrected by an elastic baseline and vector-normalized. The average spectra were calculated using Unscrambler X 10.1 software. The absorbance bands were identified and allocated from data established on pure compounds previously analysed.

2.3.3.2 Monosaccharide composition

Identification and quantification of neutral monosaccharides were performed by gas chromatography after acid hydrolysis and conversion of monomers into alditol acetates as described in Lahaye et al. (2020) (Lahaye, Falourd, Laillet, & Le Gall, 2020). Chromatography was performed on a TraceGOLD™ TG-225MS GC Column (30×0.32 mm ID) (TRACE GC Ultra Thermo Scientific™; temperature 205 °C, carrier gas H_2). For calibration, external standards and inositol as internal standard were used. Uronic acids in acid hydrolysates were quantified using the metahydroxydiphenyl colorimetric method (Blumenkr.N & Asboehan.G, 1973). All tests were done in triplicate.

2.3.4 Linkage analyses

Glycosidic linkage analyses were performed using a permethylation procedure adapted from Anumula et al. (Anumula & Taylor, 1992). Polysaccharide fractions (1 mg/mL) were converted into their H^+ form by percolating the aqueous solutions with Sigma Dowex 50 WX4 resin (1 mL). After freeze-drying, 1 mg of sample was dissolved in 1 mL of DMSO. The solution was sonicated for 2 min and then left to stand for 30 min before adding 1 mL of NaOH-DMSO reagent followed by 500 µL of methyl iodide. The solution was vortexed and sonicated three times for 2 min, and methylation was stopped by adding 2 mL of distilled water. Methylated polysaccharides were extracted with 2 mL of chloroform. After vigorous vortexing and brief centrifugation, the organic phase was washed three times with 4 mL of distilled water. After evaporation under a stream of air, methylated polysaccharides were hydrolysed with 2 N trifluoroacetic acid (TFA) with an internal standard at 110 °C for 90 min and then evaporated under a stream of air. The partially methylated monosaccharides were then converted to alditol acetates and analysed by gas chromatography/mass spectrometry (GC/MS) (TRACE-GC-ISQ, Thermo Scientific™, Waltham, Massachusetts, USA) on a nonpolar Thermo Scientific™ TraceGOLD™ TG-1MS GC Column (30 m x 0.25 mm x 0.25 µm), carrier gas H_2 at 1.5 mL/min as previously described in Buffetto et al. (Buffetto et al., 2015).

2.3.5 ^{13}C Solid-state nuclear magnetic resonance (NMR)

2.3.5.1 Crystallinity and $T_{1\rho}^{H}$ measurement

Solid-state NMR spectra were registered on a Advance III spectrometer (Bruker; Bilelrica, Massachusetts, USA) on rehydrated AIM to 30 ± 1% w/w with ultrapure water. Spectra were recorded at room temperature with a spectrometer operating at a carbon frequency of 100.62 MHz. A triple resonance ^1H/X/Y CPMAS 4 mm probe was used. The magic-angle-spinning (MAS) rate was fixed at 9 kHz. CP-MAS experiments were carried out following the method described in Bourmaud et al. (Bourmaud, Siniscalco, et al., 2018). The approach of Larsson et al. was used to evaluate the cellulose I crystallinity from the deconvoluted C4 peaks in the 77-92 ppm region (Larsson, Wickholm, & Iversen, 1997). The proportion of crystalline cellulose in the different samples was determined by dividing the area of the three peaks of the crystalline region by the areas of the six peaks for the cellulose C4 region. The lateral dimensions of the fibrils (LFD) and the lateral dimensions of the fibril aggregates

(LFAD) were then estimated assuming a square cross section of cellulose microfibrils. These estimates assumed that all amorphous cellulose was on the fibril surface. The cellulosic chain width was taken as 0.57 nm (Newman, 1999). When cellulose II was detected, the model was adapted according to (Zuckerstatter, Terinte, Sixta, & Schuster, 2013).

The chemical shift, half-width and area of peaks were determined using a least-squares fitting method using Peakfit® software (Systat Software Inc., USA).

By varying the contact time □ of cross-polarization (20 points between 10 µs and 9000 µs, with an accumulation of 1024 scans per experiment), the kinetics of cross polarization were investigated. The cross-polarization kinetics were fitted using a two-reservoir model with the following formula (Kolodziejski & Klinowski, 2002):

$$I(\tau) = I_0 e^{-\tau/T_{1\rho}^{\mathrm{H}}} * \left\{1 - \lambda e^{-\tau/T_{\mathrm{HH}}} - (1-\lambda) e^{-3\tau/2T_{\mathrm{HH}}} e^{-\tau^2/2T_{\mathrm{CH}}^2}\right\}$$

where $I(\tau)$ is the area of the carbon peak according to the contact time, I_0 is the maximum carbon signal intensity (associated with the optimal contact time), λ is a parameter that depends on the number of protons (n) carried by carbons (λ=1/(n+1)), T_{CH} is the mean dipolar coupling between carbon and proton covalently linked, T_{HH} is the spin diffusion between the two proton reservoirs, and $T_{1\rho}^{H}$ is the proton spin–lattice relaxation time in the rotating frame.

2.3.5.2 Time domain NMR (relaxometry)

In the present study, the transverse relaxation times of water protons (T_{2i}) and their associated populations (P_{2i}) were evaluated. The samples were immersed for 3 days in ultrapure water, and then the excess water was removed to fill all the cavities with water. After measurement, the water content was determined to be equal to 81 ± 5%. The acquisitions were carried out using the Carr–Purcell–Meiboom–Gill (CPMG) sequence at 4 °C. The echo time was 0.08 ms, 10000 echoes were collected, and 64 scans were acquired with a recycle delay of 7 s, resulting in a total acquisition time of approximately 20 min. An inverse Laplace transformation (ILT) was applied to convert the relaxation signal into a continuous distribution of relaxation components. For this purpose, a numerical optimization method was used, including nonnegativity constraints and L1 regularization and by applying a convex optimization solver

primal–dual interior method for convex objectives (PDCO) (Lahaye, Bouin, Barbacci, Le Gall, & Foucat, 2018) (Saunders, A., Maes, Akle, & Zahr, 2002).

3 Results

3.1 Sequential extraction: extracted fraction microscopic images

The yields for the different solvent extractions are given in Table 1. AIM is the flax bundles recovered after alcohol extraction and accounted for 99.8% of the initial dry weight of the flax bundle, only 0.2% of alcohol soluble material was removed at this step. The oxalate extract (OXAM) represents 2.75% of the AIM dry weight, with total polysaccharides accounting for 73% of the extract dry mass. The extraction with LiCl and KOH yielded approximately 5 and 2% of the AIM dry weight, respectively. While the LiCl extract contained mainly polysaccharides, total polysaccharides in the NaOH extract accounted for only 50% of its mass.

Table 1. Yield and total monosaccharide content of fractions obtained from the different extractions. * AIM accounted for 99.8% of initial dry mass

Solvent treatment	Extracted fraction % of the initial dry matter mass of flax bundles	Polysaccharide % of the extracted fraction
AIM	≤. 0.2*	na
OXAM	2.75	73.1
LiCl	5.08	68.6
KOH	2.05	50.5
AW	0.55	na

SEM was applied to the flax fibres bundles to reveal changes induced by the different extraction stages (Figure 2). For native and AIM-treated bundles, the middle lamella is very clearly visible and surrounds the flax fibres within the fibre bundles. As the sequential extraction progresses, the middle lamella is being less visible until it disappears completely. The fibre bundle is apparently still cohesive with a smoother outer surface, which effectively suggests that the middle lamella is only partially removed after pectin extraction by oxalate (OXAM). After the KOH stage, there was no longer trace of the middle lamella. The disappearance of the middle lamella is accompanied by the individualization of flax fibres. At the OXAM stage, the fibres are

still stuck together thanks to the remnants of the middle lamella. For KOH and the final acidified treated bundles, the elementary fibres are visibly detached from one another. Furthermore, at this final stage, they show a less rough surface compared to fibres in the treated bundles from the previous extraction stages.

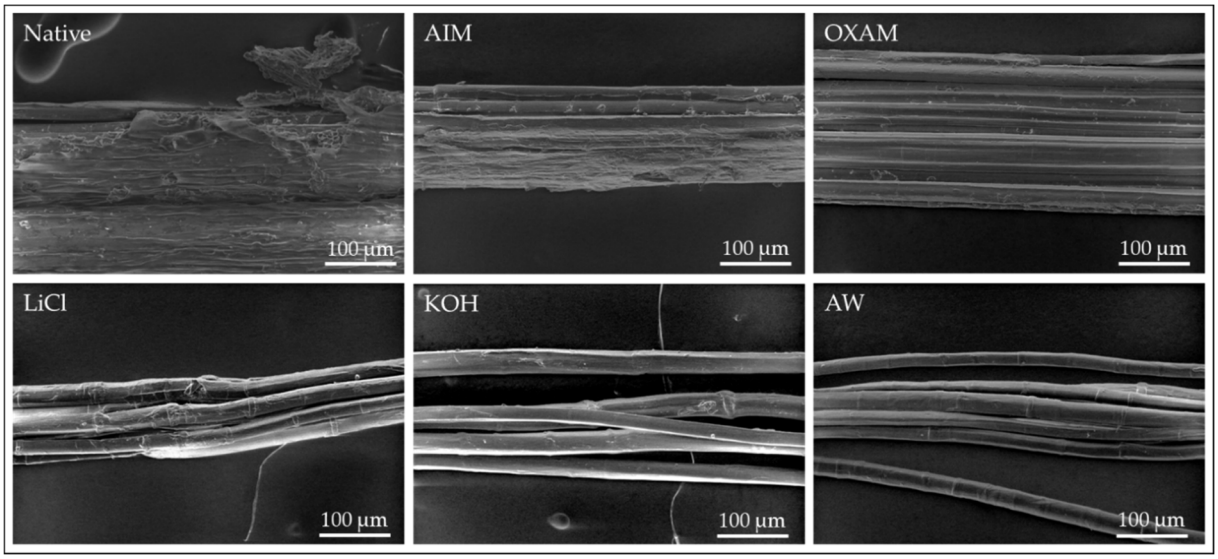

Figure 2. SEM images of each stage of the sequential extraction (×350)

3.2 Mechanical characterization of the bundles

Tensile tests on bundles were performed on the native flax and the treated bundles of the sequential extraction. Figure 3 shows the evolution of tensile strength, Young's modulus and elongation at break for the native and solvent successively extracted samples. Figure 3d confirms that our bundle tensile strength values are in the same range as the literature data, considering similar gauge lengths (Bourmaud, Nuez, Goudenhooft, & Baley, 2020). A marked and regular decrease in Young's modulus (Figure 3a) is observed as the sequential extraction progresses between AIM and LiCl. For the tensile strength at max of the fibre bundle (Figure 3b), a regular decrease is also observed up to the LiCl stage, but the high standard deviations do not allow us to make any comments.

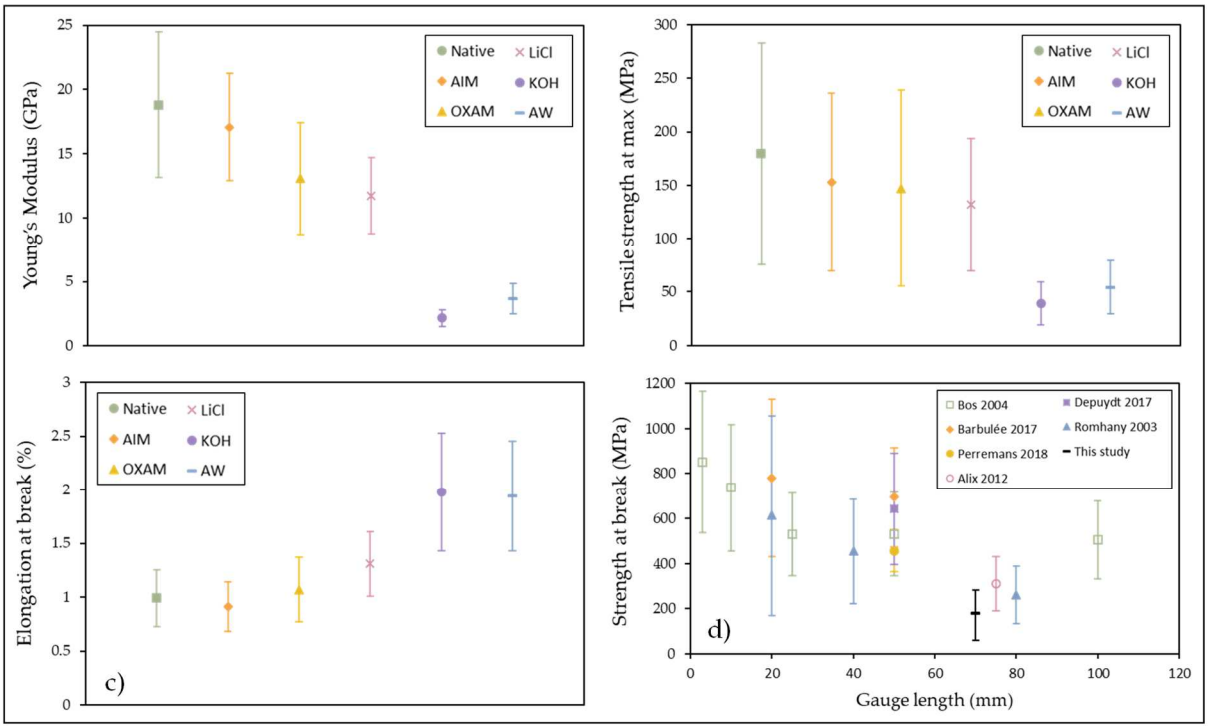

Figure 3. Evolution of the tensile mechanical properties according to the stages of sequential extraction for a gauge length of 70 mm: a) Young's modulus; b) Tensile strength at max; c) Strain at break, and d) Influence of gauge length on the strength at break (Bos, 2004) (Depuydt, Hendrickx, Biesmans, Ivens, & Van Vuure, 2017) (Romhany, Karger-Kocsis, & Czigany, 2003) (Barbulee & Gomina, 2017) (Perremans, Hendrickx, Verpoest, & Van Vuure, 2018) (Alix et al., 2012)

Regarding Young's modulus, the regular decrease was correlated with the extraction of pectin and the loosely bound hemicellulose stage (H1, LiCl). Extraction of the strongly bound hemicelluloses (KOH) results in a 5-fold decrease in Young's modulus and a 3-fold decrease in tensile strength, suggesting that not only the middle lamella but also the intrinsic structure of the flax cell walls is affected and degraded, even if this is not clearly visible through SEM observations. Regarding the elongation at break (Figure 3c), no change was observed following extraction of pectin by OXAM. Extraction of hemicelluloses induces an increase in the elongation at break by 23% and 86% for the LiCl and KOH stages, respectively.

3.3 Study of the chemical composition of bundles and extracts

3.3.1 Mid-infrared spectroscopy

Figure 4a shows the spectra of the treated bundles at the different stages of sequential extraction. The native and AIM-treated bundles show relatively close spectra, except in the regions at approximately 1730-1720 cm^{-1} after alkaline treatment, which is at a frequency between the frequencies of the C=O band in acid and ester pectin and the C=O band of acetyl groups. A decrease in the band at 1245 cm^{-1} corresponding to the C-C-O stretching band for esters can also be noted. The band at 1640 cm^{-1} is most likely due to residual water (Synytsya, Čopíková, Matějka, & Machovič, 2003) (Kacurakova, Capek, Sasinkova, Wellner, & Ebringerova, 2000). This relative absence of contrast between treated bundle samples can be explained by two reasons: i) the high cellulose content of the polysaccharide fraction, and ii) the relatively modest quantity of solubilized material during the different extraction stages.

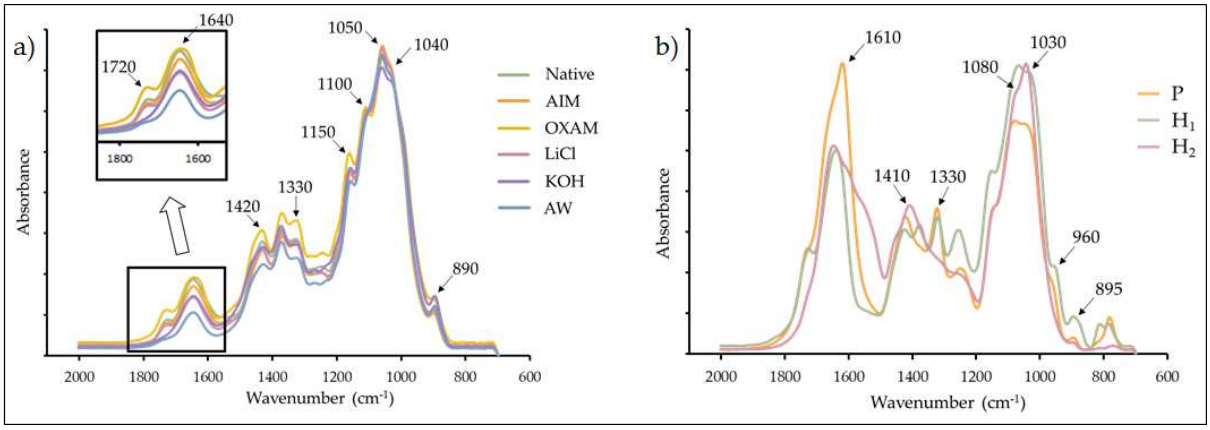

Figure 4. Fourier transform infrared (FTIR) spectra of: a) the AIM and subsequent treated bundles; and b) extracts obtained from the sequential extraction

The three extracts were analysed to obtain further information on the solubilized compounds at each extraction stage (Figure 4b). The spectra of the oxalate extract are characterized by high absorption bands at 1610 cm^{-1} with a weaker accompanying band at 1430 cm^{-1} corresponding to the antisymmetric and symmetric C=O stretching vibrations of the nonesterified carboxyl group COO^-, suggesting the presence of pectins, mainly in the salt form (Himmelsbach, 2002; Synytsya et al.,

2003). The shoulder at approximately 1738 cm^{-1} corresponds to C=O in acid, ester pectins or acetyl groups (Himmelsbach, 2002). Another band related to in-plane carboxylate bending is present at 960 cm^{-1}. The band at 1320 cm^{-1} corresponds to a non- or weakly methylated pectin, while the band at approximately 1250 cm^{-1} may be assigned to the C-C-O of acetyl groups. In the region between 1200 and 750 cm^{-1}, two main band maxima located at 1076 and 1043 cm^{-1} can be identified. The band at 1043 cm^{-1} could be assigned to arabinose containing polysaccharides, while the band at 1076 cm^{-1} could be related to galactans side chains of rhamnogalacturonans type galactose containing polysaccharides (Kacurakova et al., 2000). These two bands could be related to arabinans, galactans or arabinogalactans (Kacurakova et al., 2000) (Zhou, Sun, Bucheli, Huang, & Wang, 2009). In summary, the OXAM extract is composed mainly of low methylated HG/RG-I, with arabinans and galactans or arabinogalactans as side chains. The LiCl extract in the region between 1200-750 cm^{-1} is characterized by two maxima at 1035 cm^{-1} and 1062 cm^{-1}. The band at 1035 cm^{-1} is assigned to C-C stretching and C-O bending vibrations of glucose-containing polysaccharides, while the bands at approximately 1066 and 1080 cm^{-1} are associated with mannose and galactose units, respectively (Kacurakova et al., 2000). The band at 815 cm^{-1} is assigned to the CH bending out of plane and confirms the presence of mannans. The 956 cm^{-1} band can be attributed to pectins (Synytsya et al., 2003) can also be due to presence of highly substituted xylans (Robert, Marquis, Barron, Guillon, & Saulnier, 2005). The band at 1265 cm^{-1} associated with the bands at 1720 cm^{-1} and 1370 cm^{-1} suggests the presence of esterified methyl or acetyl groups. In conclusion, the LiCl extract is composed mainly of a hemicellulosic fraction enriched in acetylated galacto(gluco)mannans. The spectrum of the KOH fraction is characterized by carboxylate bands at 1610 and 1415 $cm^{-1,}$ suggesting the presence of pectins and amide I and II absorption bands at approximately 1645 (C=O and C-N) and 1540 cm^{-1} (C-N, N-H), respectively (Zhou et al., 2009). The band at 1720 cm^{-1} corresponding to esterified carboxyl groups is not present, as expected. In the region between 1200 and 750 cm^{-1}, two maxima at approximately 1040 cm^{-1} and 1074 cm^{-1} can be identified, which may refer to arabinose-, rhamnose- and/or xylose-containing polysaccharides and galactose-containing polysaccharides, respectively. Thus, KOH extract contains a mixture of polymers composed of pectins, hemicellulosic compounds and proteins.

To gain more insight into polysaccharide composition and structure, treated bundles and extracts were analysed for monosaccharide composition, and extracts were also subjected to methylation analysis to identify the main linkages present.

3.3.2 Monosaccharide composition

The monosaccharide composition of native flax as well as of the treated bundles and extracts was determined (Table 2).

Table 2. Chemical composition (standard deviation) of the native flax, AIM, subsequent treated bundles and extracts obtained from the different extractions. Total monosaccharides are expressed as % of dry matter (PS = Yield x Total monosaccharides/100), and neutral monosaccharide composition is expressed as weight % of total monosaccharides (NQ = not quantifiable)

Treated bundles	Total monosaccharides ($dw_{residue}$%)	Neutral and acid monosaccharide composition (total monosaccharides %)								PS (dw%)
		Rhamnose	Fucose	Arabinose	Xylose	Mannose	Galactose	Glucose	Uronic Acid	
AIM	92.7 ± 0.4	1.1 ± 0.1	NQ	1.1 ± 0.2	1.3 ± 0.1	4.3 ± 0.1	4.4 ± 0.1	84.6 ± 0.7	3.1 ± 0.2	-
OXAM	92.6 ± 4.8	1.0 ± 0.1	NQ	0.9 ± 0.2	1.2 ± 0.2	4.2 ± 0.2	4.1 ± 0.2	86.1 ± 4.2	2.4 ± 0.2	-
LiCl	82.2 ± 0.6	0.9 ± 0.1	NQ	0.8 ± 0.1	0.6 ± 0.1	2.6 ± 0.1	3.7 ± 0.1	89.0 ± 0.9	2.6 ± 0.1	-
KOH	86.3 ± 2.8	0.8 ± 0.1	NQ	0.6 ± 0.1	0.4 ± 0.1	2.4 ± 0.1	3.3 ± 0.1	90.3 ± 2.9	2.1 ± 0.1	-
AW	84.1 ± 2.8	0.9 ± 0.1	NQ	0.7 ± 0.2	0.5 ± 0.1	2.4 ± 0.1	3.3 ± 0.1	90.0 ± 2.9	2.3 ± 0.1	-
Extracts										
P	73.1 ± 5.0	2.9 ± 0.3	0.5 ± 0.2	6.5 ± 0.1	1.4 ± 0.1	3.9 ± 0.3	19.4 ± 1.0	7.0 ± 3.9	58.4 ± 5.0	2.0
H_1	68.6 ± 3.8	1.8 ± 0.3	0.5 ± 0.1	2.3 ± 0.2	8.7 ± 0.2	37.9 ± 1.6	8.2 ± 0.6	29.2 ± 0.6	11.4 ± 3.8	3.5
H_2	50.5 ± 4.8	2.9 ± 0.1	0.5 ± 0.2	8.2 ± 0.6	8.5 ± 0.6	5.2 ± 0.4	21.0 ± 1.2	27.0 ± 0.9	26.7 ± 5.0	1.0

In the AIM-treated bundles, total monosaccharides accounted for 92.6% of the dry matter. Glucose (84.6%) was the main monosaccharide, followed by galactose (4.4%), mannose (4.3%) and uronic acid (3.1%). Arabinose, xylose and rhamnose are present in small amounts (less than 2% of dry matter). The AIM-treated bundles exhibit a monosaccharide composition very close to the monosaccharide composition of native flax (not shown), in agreement with this stage aiming mainly at inactivating endogenous enzymes and removing the few impurities, such as waxes and oils, present at the surface of the flax fibres. The OXAM-treated bundles showed little

variation in monosaccharide composition compared to AIM-treated bundles. Only the level of uronic acids decreased from 3.1% to 2.4%. The OXAM extract (P), for which total monosaccharide accounts for 73.1% of the dry matter, is composed mainly of uronic acids (58.4%), followed by galactose (19.4%), glucose (7.0%) and arabinose (6.5%). In contrast, LiCl-treated bundles showed some changes in monosaccharide composition. Total monosaccharide accounted for 68.6% of the dry matter of the LiCl extract (H_1), which is particularly rich in mannose (37.9%) followed by glucose (29.2%). Xylose, Galactose and uronic acids are also present in smaller amounts. The final KOH stage aims at removing more strongly bound hemicelluloses. The monosaccharide composition of KOH-treated bundles was very close to the monosaccharide composition of the LiCl-treated bundles for all neutral monosaccharides. A decrease in uronic acids was observed from 2.6% to 2.1% at the KOH stage. The composition of the KOH extract (H_2) differs significantly from the composition of the LiCl extract (H_1). Total monosaccharides accounted for only 50.5% of the dry mass. H_1 is rich in glucose (27.0%), uronic acids (26.7%), galactose (21.0%), xylose (8.5%) and arabinose (8.2%), and mannose is present in lower amounts (5.2%). The AW-treated bundles showed no difference in monosaccharide composition when compared to the KOH-treated bundles.

3.3.3 Determination of polysaccharide glycosidic linkages

To obtain further information on the cell wall polysaccharides present in the P, H_1 and H_2 extracts, glycosidic linkage analyses were performed. Compositional analyses revealed that HG was the main polysaccharide in the P extract. The linkage analyses show relatively high contents of (1,2)-linked Rha (3.2%) and of (1,2,4)-linked Rha (2.2%) together with (1-4)-linked Gal (16%) and (1-5)-linked Ara (29.1%), suggesting that RG-I domains are substituted by linear 1,4-galactan and 1,5-arabinan side chains in this extract (T. Gorshkova & C. Morvan, 2006). The presence of type II arabinogalactans (AG-II) is also revealed, thanks to the detection of (1,3)-, (1,6)- and (1,3,6)-linked Gal (4, 1.2 and 0.6%, respectively) and t-Ara (15.2%) (Pettolino, Walsh, Fincher, & Bacic, 2012). Glucose appears predominantly in the (1,4)-linked form, and xylose appears as unsubstituted (1,4)-linked Xyl. The non-detection of (1,4,6)-linked Glc and t-Xyl suggests the absence of xyloglucans (XG) (McDougall, 1993).

462 **Table 3. Glycosidic linkages of neutral monosaccharides from the different**
463 **fractions: P, H1 and H2**

Linkages	P		H_1		H_2	
	% Total sugar	Proportion per monosacch. type	% Total sugar	Proportion per monosacch. type	% Total sugar	Proportion per monosacch. type
t-Rha	1.9	24.3				
2-Rha	3.2	41.0	0.6	66.7	2.3	71.9
2,4-Rha	2.2	28.2	0.3	33.3	0.8	28.1
2,3,4-Rha	0.6	7.7				
TOTAL	**7.8**	**100%**	**0.9**	**100%**	**3.2**	**100%**
t-Xyl			3.0	18.5	4.0	9.5
4-Xyl	4.1	100.0	13.3	81.5	29.9	70.7
2-Xyl					8.3	19.8
TOTAL	**4.1**	**100%**	**16.2**	**100%**	**42.3**	**100%**
t-Gal	10.1	31.7	3.2	80.0	5.5	52.9
3-Gal	4.0	12.5	0.8	20.0	2.4	23.1
4-Gal	16.0	50.2				
6-Gal	1.2	3.8				
3,6-Gal	0.6	1.8			2.1	20.2
3,4,6-Gal					0.2	1.9
TOTAL	**31.9**	**100%**	**4.0**	**100%**	**10.4**	**100%**
t-Ara	15.2	34.2	0.1	25.0	6.8	100.0
5-Ara	29.1	65.8	0.3	75.0		
TOTAL	**44.4**	**100%**	**0.4**	**100%**	**6.8**	**100%**
t-Glc	1.8	17.8	1.2	3.1	1.5	5.5
3-Glc					4.6	16.8
4-Glc	8.3	82.2	35.6	90.8	19.3	70.4
4,6-Glc			2.4	6.1	2.0	7.3
TOTAL	**10.1**	**100%**	**39.2**	**100%**	**27.4**	**100%**
t-Man	0.7	100.0	1.2	3.1	0.5	8.5
4-Man			37.7	96.2	5.4	91.5
4,6-Man			0.3	0.7		
TOTAL	**0.7**	**100%**	**39.2**	**100%**	**5.9**	**100%**

464

In the H_1 extract, (1,4)-linked Man (37.3%), (1,4,6)-linked Man (0.3%), t-Gal (3.2%) and (1,4)-linked Glc (35.6%) suggest the presence of galactomannans (Lefeuvre, Baley, & Morvan, 2018) and/or gluco(galacto)mannans (Charlet et al., 2007), weakly branched at O6 with galactose. The presence of (1,4)-linked Glc, (1,4,6)-linked Glc (2.4%) and t-Xyl (3.0%) indicates the presence of xyloglucans (Pettolino et al., 2012), while (1,4)-linked Xyl (13.3%) indicates the presence of xylan (Rihouey, Paynel, Gorshkova, & Morvan, 2017). RG-I is also detected in low amounts according to (1,2)-linked Rha (0.6%) and (1,2,4)-linked Rha (0.3%) (Pettolino et al., 2012). H_1 extract is composed mainly of hemicelluloses with glucomannans as the main polysaccharides.

In the H_2 fraction, (1,4)-linked Glc (19.3%), (1,4,6)-linked Glc (2.0%), (1-2)-linked Xyl (8.3%), t-Gal (5.5%) and t-Xyl (4.0%) indicate the presence of XG (Pettolino et al., 2012). The (1,3)-linked Gal (2.4%) and (1,3,6)-linked Gal (0.2%) bonds attest to the presence of AG-II (T. Gorshkova & C. Morvan, 2006). Galactose, which is the second main monosaccharide in H_2 as determined by direct monosaccharide analysis, is underrepresented in the monosaccharide linkages analysis because galactose may be associated with a polymer that is poorly soluble in DMSO. The extract also contained low substituted (1,4)-linked xylan. H_2 extracts contained hemicellulosic polysaccharides, mainly xylans and xyloglucans, residual pectins and AG II.

3.4 Structural analysis of flax cellulose along sequential extraction

The internal structure of the flax fibres was probed by ssNMR to observe the possible impacts of the different stages of the extraction. Figure 5 shows the annotated ^{13}C

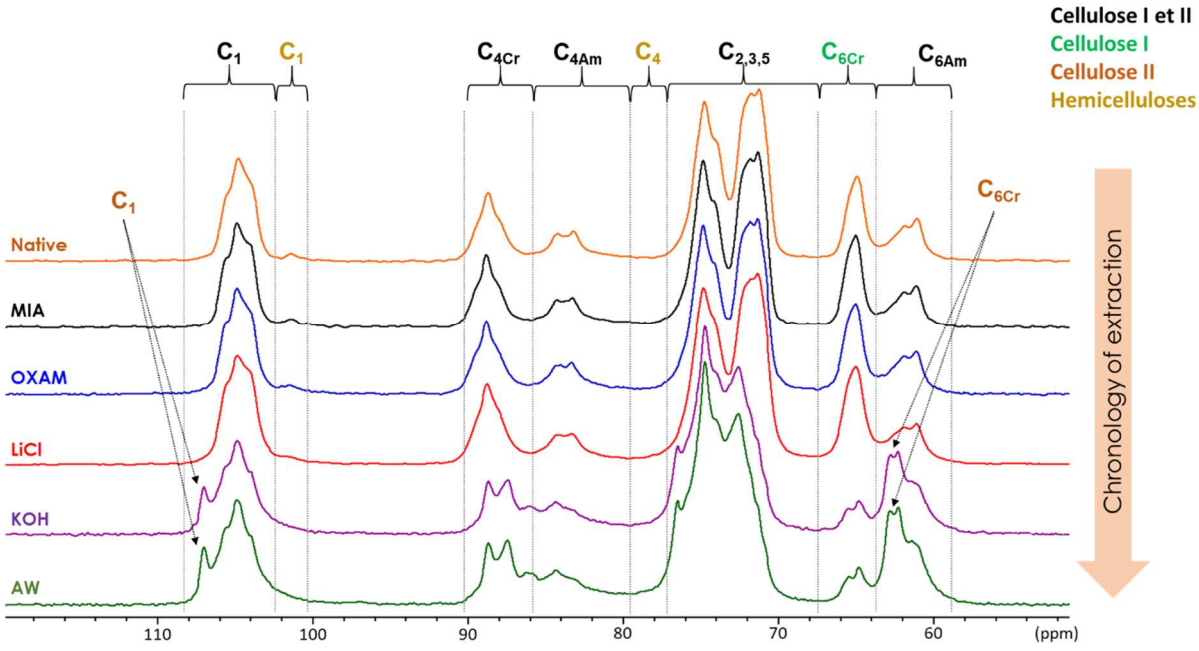

CP/MAS spectra of the treated bundles after the fifth sequential extraction stages.

Figure 5. Annotated ^{13}C CP/MAS spectra of the stages of sequential extraction (cr = crystalline and am = amorphous)

Carbon numbers refer to anhydroglucose structural elements. For the native flax-, AIM, oxalate- and LiCl-treated bundles, there were no differences in the chemical shifts of the spectra regardless of the carbon considered. The spectra correspond to cellulose I spectra (Newman & Davidson, 2004). In contrast, new peaks appear in the KOH-treated bundles. Indeed, for C_1, C_{4cr} and C_6, the new peaks indicate the presence of cellulose II (Newman & Davidson, 2004). The appearance of cellulose II is characteristic of a reorganization of the structure of the sample. KOH treatment is therefore similar to a mercerization treatment (Zuluaga et al., 2009). A decrease in the intensity of the spectrum is observed for C_1 relating to hemicelluloses for the LiCl and KOH stages.

The deconvolution of the C_4 area was carried out to obtain additional information (Table 4) on cellulose crystallinity. Native flax has a crystallinity of 58% with an LFD and an LFAD equal to 4.8 and 17.4 nm, respectively. For the AIM, only the LFAD parameter differs from native flax with a decrease of approximately 33%. This result is explained by the appearance of the collapse phenomenon following the alcoholic extraction stage. The apparent crystallinity in OXAM-treated bundles shows a decreasing trend, from 59% to 57% for AIM and OXAM, respectively. In contrast, an increasing trend is observed for the LiCl extraction, which suggests a coextraction of amorphous cellulose with hemicelluloses. In the KOH-treated bundles, the generation of cellulose II was accompanied by a significant reduction (20%) in crystallinity. The AW treatment does not induce additional changes. Except after OXAM treatment, LFAD decreases during extractions, suggesting a gradual decrease in the porosity of the samples. In other words, the distance separating two fibrils decreases. The LFAD/LFD ratios are the same throughout the sequential extraction, except for the OXAM stage, indicating that an aggregate is always composed of the same number of fibrils. The C_6 area has also been deconvoluted to obtain additional information. In KOH- and AW-treated bundles, cellulose II accounted for 66% and cellulose I accounted for 34% of the total cellulose. This change in cellulose conformation explains the drop in the crystallinity observed in the KOH-treated bundles.

Table 4. Different calculated parameters of C_4 area and the $T_{1\rho}^{H}$ parameter for the crystalline C_4

Sample	Crystallinity	LFD (nm)	LFAD (nm)	LFAD / LFD	$T_{1\rho}{}^{H}$ (ms)
Native	58%	4.8	17.4	3.6	49
AIM	59%	4.9	11.9	2.4	60
OXAM	57%	4.7	14.2	3.0	190
LiCl	61%	5.2	11.5	2.2	196
KOH	49%	3.8	9.7	2.6	22
AW	50%	3.9	8.9	2.3	70

Sequential extraction caused significant changes in the bundle composition with the removal of a large part of the matrix polysaccharides, which may have caused some changes in the cellulose environment. We assessed the cellulose environment through $T_{1\rho}^{\mathrm{H}}$ relaxation (Table 4, last column) measurements of crystalline cellulose C4 (87-90 ppm). The T_{CH} and T_{HH} parameters are not shown in this study due to the absence of notable differences between the different samples. Thus, only the $T_{1\rho}^{\mathrm{H}}$ was analysed, the observed differences of the $T_{1\rho}^{\mathrm{H}}$ are summarized in Table 4. $T_{1\rho}^{\mathrm{H}}$ increases with the molecular order and rigidity of the structure. For crystalline C_4, some changes in values are observed during all sequential extractions, especially with higher absolute values, which illustrates the link between the value of $T_{1\rho}^{\mathrm{H}}$ and the level of molecular order. There is a strong increase in $T_{1\rho}^{\mathrm{H}}$ at the OXAM stage characteristic of the elimination of amorphous polymers. The KOH stage shows a drastic decrease in $T_{1\rho}^{\mathrm{H}}$, from 196 ms for the LiCl-treated bundles to 22 ms for the KOH stage-treated bundles. In addition to the decrease in the order reflected by the decrease in $T_{1\rho}^{\mathrm{H}}$, the notion of heterogeneity, corresponding to a form of disorder, should be considered. Indeed, at this stage of sequential extraction, cellulose II appears. However, the rinsing stages led to an increase in $T_{1\rho}^{\mathrm{H}}$. The AW stage may have removed some soluble substances, which may have caused the cellulose microfibrils to be closer together and more organized.

Information on interactions between water and biomass at the molecular level was collected using TD-NMR. The distribution of water mobility in the flax samples was characterized by analysis of the T_2 relaxation time. Each T_2 peak can be preferentially assigned to a pool of water at a given range of mobilities corresponding to a specific molecular environment/interaction (Figure 6).

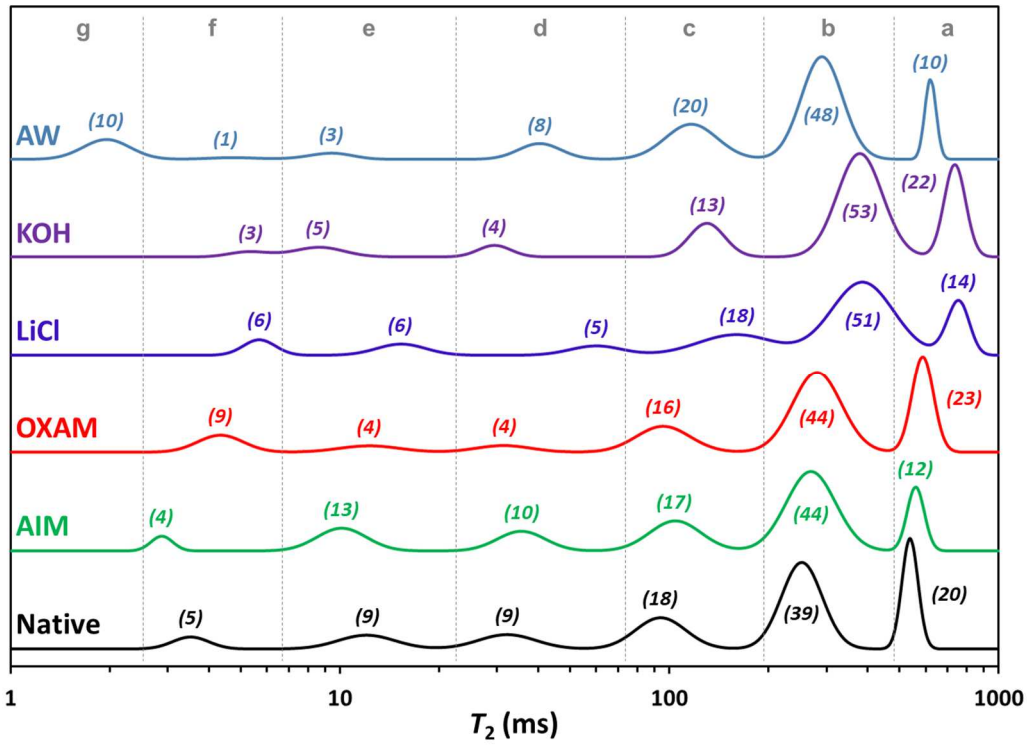

Figure 6. T_2 relaxation time distributions for extraction stages. The normalized populations associated with each water environment (noted at the bottom with grey letters) are mentioned in parenthesis.

Between 6 and 7 distinct T_2 peaks are visible for all samples. The peaks are noted from *a* (longest relaxation time) to *g* (smallest relaxation time). Each $T_{2\mathrm{i}}$ relaxation time is associated with a proportion of water $P_{2\mathrm{i}}$ (Supplementary Data 2).

For the Native sample, six populations of water were identified covering a wide range of relaxation times: from short $T_{2\mathrm{g}}$ (3.5 ms) to long $T_{2\mathrm{a}}$ (537 ms). The AIM and OXAM T_2 times and water populations were close to the T_2 times and water populations of the native sample. The longest relaxation times $T_{2\mathrm{a}}$ and $T_{2\mathrm{b}}$ (573 and 275 ms,

561 respectively) accounted for 61.5% of the total water content, assigned to less
562 constrained water. The pool of water associated with intermediate component $T_{2c,d,e}$
563 accounted for 26.5% of the total water content. A small shift towards a higher water
564 mobility mode was observed for the shortest T_{2f} time (4.3 ms) for OXAM. This pool of
565 water corresponded to more constrained water and accounted for 9% of the total
566 water content. In contrast, extraction of hemicelluloses by LiCl and KOH leads to a
567 shift towards high modes for T_{2a} (742 ms) and T_{2b} (381 ms), accounting for 70%,
568 which could partially result from swelling. This tendency was reversed by acidic
569 treatment with 620 ms and 290 ms for T_{2a} and T_{2b}, respectively. These pools of water
570 accounted for 57% of the total water content. The pool of more constrained water
571 corresponding to T_{2e}, T_{2f} and T_{2g} times (9, 5 and 2 ms, respectively) accounted for
572 14% of the total water.

573 # 4 Discussion

574 In this study, the relationships between the tensile mechanical properties of flax fibre
575 bundles as well as their chemical composition and structure were investigated after a
576 sequential solvent extraction. Fibre bundles were treated as alcohol-insoluble
577 material to remove traces of components not directly in the cell wall structures but still
578 deposited on them. Pectins were first extracted by ammonium oxalate, and then
579 loosely and more strongly bound hemicelluloses were solubilized by DMSO doped
580 with LiCl and 4N KOH, respectively.

581 The AIM shows a slight decrease in mechanical properties measured by the tensile
582 test compared to native bundles. Alcoholic extraction removed mainly non-cell wall
583 compounds such as impurities and waxes from the surface of fibres. Nevertheless,
584 this stage appears to affect the fibre bundle structure, and in particular, the middle
585 lamella, which ensures the cohesion of the fibres, begins to be degraded. One
586 possible hypothesis would be the plasticization of pectins modifying the interactions
587 between the polymers without affecting the cellulose. However, the monosaccharide
588 composition of the Alcohol-treated bundles does not show significant differences from
589 native flax, suggesting that no polymer extraction has occurred at this stage. ssNMR
590 applied to treated bundles resulting from cell wall polysaccharide sequential
591 extraction is able to reveal changes induced in the cell wall network (Herbaut et al.,
592 2018) (Leroy et al., 2021). The integrity of flax fibres is confirmed by structural

analysis by ssNMR that showed no significant variation in various cellulose parameters, such as crystallinity. The sharp drop in LFAD could indicate the removal of the inaccessible surface caused by solvent exchange. At the scale of the fibre bundle, for a boiling water stage, an increase in the diameter of the fibres has been shown to be mainly caused by the sorption of the solvent and the extraction of cortically treated bundles, which can cause restructuring of the outer cell wall of the fibre (Lefeuvre et al., 2015).

Then, the OXAM-treated bundles show a decrease in both tensile Young's modulus and tensile strength. SEM images reveal a partial elimination of the middle lamella, visible at the interface between elementary fibres. From the monosaccharide composition and linkage analyses, it can be deduced that the dominant polysaccharides extracted by oxalate were pectins rich in HG and RG-I domains rich in side chains of galactans and, to a lesser extent, arabinans, rather linear. These polysaccharides have been identified in gelatinous layers (Tatyana Gorshkova & Claudine Morvan, 2006; Mellerowicz & Gorshkova, 2011), but are also are signature of the middle lamella and of the primary cell wall (Richely, Bourmaud, Placet, Guessasma, & Beaugrand, 2021), thus emphasizing their contribution during mechanical stress at the scale of the fibre bundle (Rihouey, Paynel, Gorshkova, & Morvan, 2017b). In addition, transfer loading is ensured mainly by the middle lamella when fibre bundles are mechanically stressed. The same observation has already been addressed for elementary flax fibres, suggesting the contribution of the primary wall and the residual pectins to the mechanical properties (Placet, Cisse, & Boubakar, 2014). However, at the bundle scale, the mechanical contribution of the middle lamella is very important due to its role in the cohesion of elementary fibres, especially when tensile tests with high gauge lengths are considered. At the OXAM stage, a change in trend appears to be initiated for elongation at break with an increase that will continue for the rest of the sequential extraction. The extraction of cell wall amorphous polymers is known to create discontinuities within the macromolecular network (Videcoq et al., 2017). Indeed, between the extraction and tensile tests, the fibres were dried, which could have favoured the creation of new hydrogen bonds in the cellulose-enriched fibre (Fratzl, Burgert, & Gupta, 2004). Studies have indeed hypothesized the setting of hydrogen bonds between RG-I-Gal structures and cellulose (Alix et al., 2009) based on experiments reports where *in*

626 *vivo* and *in vitro* binding competitions permit quantification of matrixial polymers on
627 cellulose, thank to time course, radiolabelling of fluorescent quantifications (Hayashi,
628 Marsden, & Delmer, 1987) Since crystallinity is not altered, OXAM stage may allow
629 the elimination of mostly amorphous polymers, which leads to an increase in the $T_{1\rho}^{H}$
630 value, suggesting a higher order level around the cellulose molecules. This removal
631 also impacts the proportion of the water population associated with $T_{2\mathrm{d}}$ and $T_{2\mathrm{e}}$
632 relaxation time, which corresponds to relatively constrained water. The sum of these
633 two intermediate water populations decreased from 23% (AIM) to 8% (OXAM), while
634 at the same time, the more mobile water population corresponding to T_{2a} and T_{2b}
635 increased due to water-cell wall interactions, which could be attributed to changes in
636 the chemical environments inside the bundles. Analysis of the elongation at break on
637 elementary fibres showed a different trend: an increase with the extraction of pectins
638 then a decrease with the extraction of hemicelluloses (Lefeuvre et al., 2015).

639 The KOH stage induces a significant drop in the mechanical properties for Young's
640 modulus and tensile strength, which are decreased by five and three compared to the
641 previous LiCl stage, respectively. This loss of mechanical properties of the extracted
642 bundles is arguably due to the successive removal of the cell-wall polymers of
643 elementary fibre, but based on the microscopic observations and polymer signatures
644 removal due to middle lamella destruction. Indeed, in our case with a gauge length of
645 70 mm, no elementary fibre could be clamped at either of its extremities. The middle
646 lamella, which holds the fibre bundles together (pectin and hemicelluloses rich), has
647 significantly weakened, resulting in a decrease in the tensile mechanical properties.
648 The monosaccharide composition of the KOH-treated bundles was close to the
649 monosaccharide composition of the LiCl bundles, with similar levels of xylose,
650 rhamnose and mannose. However, the linkage analysis of the extracts shows some
651 differences. The H_2 extract consisted mainly of hemicelluloses in the form of xylans
652 and xyloglucans but also of residual pectins and AG II, as confirmed by FTIR
653 analysis. The extraction of structural polysaccharides such as hemicelluloses
654 combined with a lack of cohesion of elementary fibre within the bundle then
655 generates weak mechanical properties at the bundle scale (Bourmaud et al., 2013).
656 After KOH extraction, the weak cohesion measured is expected to be due to
657 hydrogen bonding between the highly cellulosic fibres generated and due to physical
658 entanglement of elementary fibre within the vestige fibre bundle. For example, the

Young's modulus for an elementary flax fibre having undergone a comparable strategy of polymers extraction as done in this work is 24 GPa (Lefeuvre et al., 2015). We can arguably hypothesize that the resulting final individual fibers from Lefeuvre et al. is therefore extracted in non-cellulosic polysaccharides in a comparable way to this study. Remarkably, the Young's modulus of bundles composed of such extracted fibres (about 24 GPa) is only 3.7 GPa whereas the unextracted bundles are close to 18 GPa in this study. Because the middle lamella is the material stressed during the tensile testing, we can hypothesize that, when bundle testing is considered, the impact of the extraction of the middle lamella is largely preponderant (decrease of the Young's modulus from 18 to 3.7 GPa) compared to the impact on individual fibre (decrease from 56 to 24 GPa). In addition, the structure of the fibre is altered, as shown by NMR characterization. Indeed, during this KOH stage, many structural variations are observed: the appearance of cellulose II and a decrease in crystallinity, which could impact the intrinsic properties of flax fibre. This heterogeneity reflects a less ordered structure characterized by a lower $T_{1\rho}^{H}$ than in the LiCl stage, for example. The long relaxation times $T_{2\mathrm{a}}$ and $T_{2\mathrm{b}}$, associated with less constrained water, increased in the KOH stage but also in the LiCl stage. During these stages, the matrix polymers (hemicelluloses and pectins) and the most hydrophilic polymers are eliminated, affecting and modifying the environment around cellulose. In this way, the strong interactions of water within the microfibrils are reduced. The LFAD/LFD ratio remains unchanged throughout the sequential extraction with 3 fibrils per unit of aggregate, but it remains difficult to estimate the gap between them because of the fluctuations according to the treatments. However, the structure changes due to the change in size of the objects. In addition, a decrease in LFAD is observed at the KOH stage, meaning a decrease in the distance between the cellulose microfibrils, which could then promote the connection between the microfibrils. Indeed, after NaOH extraction, similar to KOH extraction, cellulose microfibrils have been shown to be able to connect to each other by forming a highly cohesive cellulose network (Lefeuvre et al., 2015). At the scale of elementary fibre, elongation has been shown to increase following pectin extraction, thus allowing greater elongation (O. Arnould et al., 2017), and then decrease following hemicellulose extraction. However, during mechanical tests carried out at the bundle scale, the elongation at break would be more due to easier sliding between the fibres.

5 Conclusions

A sequential extraction (AIM, OXAM, LiCl, KOH and AW) was performed at the flax fibre bundle scale to better understand the impact of the extracted cell-wall polymers on the mechanical properties, with an original focus on the middle lamella contribution. The AIM stage primarily removes surface components, particularly those characterized by a drop in LFAD, and results in a moderate drop in Young's modulus and stress induced by the start of middle lamella removal. Fewer interactions between water and cell wall polymers were observed for T_2 between 4 and 30 ms assigned to more constrained water. The linkage analysis of the P fraction associated with the OXAM stage indicates the presence of a mixture of HG, RGI and AG-II, characteristic of the middle lamella and the primary wall, although some amount can be also founded in gelatinous layer. Further removal of remnants of the middle lamella and preservation of hemicellulosic structures also results in a moderate decrease in tensile stress and Young's modulus. In addition, OXAM extraction induces changes in the cellulose environment, as highlighted by the increase in $T_{1\rho}^{H}$, while the cellulose crystallinity remains stable. Then, the H_1 fraction of the LiCl stage is composed mainly of glucomannans as well as xyloglucans relating to hemicellulosic structures. Finally, the KOH stage made it possible to extract more strongly bound hemicelluloses in the presence of XG and xylan and in the presence of residual pectins found in the H_2 fraction. A significant decrease was observed for Young's modulus and stress, divided by 5 and 3, respectively. The KOH stage also generates a profound change in the cellulose structure, as evidenced by the appearance of cellulose II and the drop in crystallinity (-20%). The presence of cellulose I and cellulose II causes a significant drop in order, divided by 9, and a huge decrease in $T_{1\rho}^{H}$, indicating more heterogeneity of the cellulose.

This work confirms the preponderant role of the middle lamella in the mechanical properties of flax fibre bundles. The elimination of the middle lamella, carried out during the first treatments, is followed by more aggressive extractants. The latter have been shown herein to cause irreversible damage to the biochemical cell wall structure. Its consequences are not visible on the scale of a mechanical characterization on bundles with a large gauge length, as is the case here, but would probably be visible within a composite in which the reinforcing fibres are embedded in the polymer matrix.

6 Acknowledgements

The authors thank Jacqueline Vigouroux, Sylviane Daniel and Lucie Le Bot for the beneficial discussions on biochemical analysis and for their support. SEM observations, glycosidic linkage and NMR analyses were performed on the BIBS instrumental platform (Biogenouest). The authors also thank the INTERREG VA FCE Program, FLOWER project, Grant Number 23, for the funding of this work.

7 References

Akin, D. E., Gamble, G. R., Morrison, W. H., Rigsby, L. L., & Dodd, R. B. (1996). Chemical and structural analysis of fibre and core tissues from flax. *Journal of the Science of Food and Agriculture,* 72(2), 155-165.

Alix, S., Goimard, J., Morvan, C., & Baley, C. (2009). *Influence of pectin structure on the mechanical properties of flax fibres: a comparison between linseed-winter variety (Oliver) and a fibre-spring variety of flax (Hermes)*. Wageningen: Wageningen Acad Publ.

Alix, S., Lebrun, L., Marais, S., Philippe, E., Bourmaud, A., Baley, C., & Morvan, C. (2012). Pectinase treatments on technical fibres of flax : Effects on water sorption and mechanical properties. *Carbohydrate Polymers,* 87, 177-185.

Anumula, K. R., & Taylor, P. B. (1992). A comprehensive procedure for preparation of partially methylated alditol acetates from glycoprotein carbohydrates. *Analytical Biochemistry,* 203(1), 101-108.

Arnould, O., Siniscalco, D., Bourmaud, A., Le Duigou, A., & Baley, C. (2017). Better insight into the nano-mechanical properties of flax fibre cell walls. *Industrial Crops and Products,* 97, 224-228.

Arnould, O., Siniscalco, D., Bourmaud, A., Le Duigou, A., & Baley, C. (2017). Better insight into the nano-mechanical properties of flax fibre cell walls. *Industrial Crops and Products,* 97(Supplement C), 224-228.

Assor, C., Quemener, B., Vigouroux, J., & Lahaye, M. (2013). Fractionation and structural characterization of LiCl-DMSO soluble hemicelluloses from tomato. *Carbohydrate Polymers,* 94(1), 46-55.

Baley, C., Goudenhooft, C., Gibaud, M., & Bourmaud, A. (2018). Flax stems: from a specific architecture to an instructive model for bioinspired composite structures. *Bioinspiration & Biomimetics,* 13(2), 12.

Barbulee, A., & Gomina, M. (2017). *Variability of the mechanical properties among flax fiber bundles and strands*. In R. Fangueiro (Ed.), *3rd International Conference on Natural Fibers: Advanced Materials for a Greener World, Icnf 2017* (pp. 487-493). Amsterdam: Elsevier Science Bv

Blumenkr.N, & Asboehan.G. (1973). New method for quantitative determination of uronic acids. *Analytical Biochemistry,* 54(2), 484-489.

763 Bos, H. (2004). The potential of flax fibers as reinforcement for composite materials.
764 Technische Universiteit Eindhoven.
765 Botany of flax. (1952). *Nature,* 170, 557-559.
766 Bourmaud, A., Beaugrand, J., Shah, D. U., Placet, V., & Baley, C. (2018). Towards the
767 design of high-performance plant fibre composites. *Progress in Materials*
768 *Science,* 97, 347-408.
769 Bourmaud, A., Morvan, C., Bouali, A., Placet, V., Perré, P., & Baley, C. (2013).
770 Relationships between micro-fibrillar angle, mechanical properties and
771 biochemical composition of flax fibers. *Industrial Crops and Products,* 44, 343-
772 351.
773 Bourmaud, A., Nuez, L., Goudenhooft, C., & Baley, C. (2020). *Multi-scale mechanical*
774 *characterization of flax fibres for the reinforcement of composite materials*. In
775 *Handbook of Natural Fibres (Second Edition)* (pp. 205-226): The Textile Institute
776 Book Series
777 Bourmaud, A., Shah, D. U., Beaugrand, J., & Dhakal, H. N. (2020). Property changes
778 in plant fibres during the processing of bio-based composites. *Industrial Crops*
779 *and Products,* 154, 14.
780 Bourmaud, A., Siniscalco, D., Foucat, L., Goudenhooft, C., Falourd, X., Pontoire, B., . .
781 . Baley, C. (2018). Evolution of flax cell wall ultrastructure and mechanical
782 properties during the retting step. *Carbohydrate Polymers*.
783 Buffetto, F., Cornuault, V., Rydahl, M. G., Ropartz, D., Alvarado, C., Echasserieau, V.,
784 . . . Guillon, F. (2015). The deconstruction of pectic rhamnogalacturonan I
785 unmasks the occurrence of a novel arabinogalactan oligosaccharide epitope.
786 *Plant and Cell Physiology,* 56(11), 2181-2196.
787 Charlet, K., Baley, C., Morvan, C., Jernot, J. P., Gomina, M., & Breard, J. (2007).
788 Characteristics of Hermes flax fibres as a function of their location in the stem
789 and properties of the derived unidirectional composites. *Composites Part a-*
790 *Applied Science and Manufacturing,* 38(8), 1912-1921.
791 Charlet, K., & Beakou, A. (2011). Mechanical properties of interfaces within a flax
792 bundle - Part I: Experimental analysis. *International Journal of Adhesion and*
793 *Adhesives,* 31(8), 875-881.
794 Coimbra, M. A., Barros, A., Rutledge, D. N., & Delgadillo, I. (1999). FTIR
795 spectroscopy as a tool for the analysis of olive pulp cell-wall polysaccharide
796 extracts. *Carbohydrate Research,* 317(1-4), 145-154.
797 Depuydt, D., Hendrickx, K., Biesmans, W., Ivens, J., & Van Vuure, A. W. (2017).
798 Digital image correlation as a strain measurement technique for fibre tensile
799 tests. *Composites Part a-Applied Science and Manufacturing,* 99, 76-83.
800 Diederichsen, A., & Hammer, K. (1995). Variation of cultivated flax (Linum
801 usitatissimum L. subsp.usitatissimum) and its wild progenitor pale flax
802 subsp.angustifolium (Huds.) Thell.). *Genetic Resources and Crop Evolution,*
803 42(3), 263-272.

804 Fratzl, P., Burgert, I., & Gupta, H. S. (2004). On the role of interface polymers for the
805 mechanics of natural polymeric composites. *Physical Chemistry Chemical*
806 *Physics*, 6(24), 5575-5579.
807 Fu, S. Y., Lauke, B., Mäder, E., Yue, C. Y., & Hu, X. (2000). Tensile properties of short-
808 glass-fiber and short-carbon-fiber-reinforced polypropylene composites.
809 *Composites Part A: Applied Science and Manufacturing*, 31(10), 1117-1125.
810 Gorshkova, T., Chernova, T., Mokshina, N., Ageeva, M., & Mikshina, P. (2018). Plant
811 'muscles': fibers with a tertiary cell wall. 218(1), 66-72.
812 Gorshkova, T., Chernova, T., Mokshina, N., Gorshkov, V., Kozlova, L., & Gorshkov,
813 O. (2018). Transcriptome Analysis of Intrusively Growing Flax Fibers Isolated
814 by Laser Microdissection. *Scientific Reports*, 8(1), 14570.
815 Gorshkova, T., Mokshina, N., Chernova, T., Ibragimova, N., Salnikov, V., Mikshina,
816 P., . . . Mellerowicz, E. J. (2015). Aspen Tension Wood Fibers Contain β-(1→4)-
817 Galactans and Acidic Arabinogalactans Retained by Cellulose Microfibrils in
818 Gelatinous Walls. *Plant physiology*, 169(3), 2048.
819 Gorshkova, T., & Morvan, C. (2006). Secondary cell-wall assembly in flax phloem
820 fibres: role of galactans. *Planta*, 223(2), 149-158.
821 Gorshkova, T., & Morvan, C. (2006). Secondary cell-wall assembly in flax phloem
822 fibres: role of galactans. *Planta*, 223(2), 149-158.
823 Gorshkova, T. A., Gurjanov, O. P., Mikshina, P. V., Ibragimova, N. N., Mokshina, N.
824 E., Salnikov, V. V., . . . Chemikosova, S. B. (2010). Specific type of secondary
825 cell wall formed by plant fibers. *Russian Journal of Plant Physiology*, 57(3), 328-
826 341.
827 Gorshkova, T. A., Wyatt, S. E., Salnikov, V. V., Gibeaut, D. M., Ibragimov, M. R.,
828 Lozovaya, V. V., & Carpita, N. C. (1996). Cell-wall polysaccharides of
829 developing flax plants. *Plant Physiology*, 110(3), 721-729.
830 Goubet, F., Bourlard, T., Girault, R., Alexandre, C., Vandevelde, M. C., & Morvan, C.
831 (1995). Structural features of galactans from flax fibers. *Carbohydrate Polymers*,
832 27(3), 221-227.
833 Goudenhooft, C., Siniscalco, D., Arnould, O., Bourmaud, A., Sire, O., Gorshkova, T.,
834 & Baley, C. (2018). Investigation of the mechanical properties of flax cell walls
835 during plant development: The relation between performance and cell wall
836 structure. *Fibers*, 6(1), 9.
837 Gourier, C., Le Duigou, A., Bourmaud, A., & Baley, C. (2014). Mechanical analysis of
838 elementary flax fibre tensile properties after different thermal cycles.
839 *COMPOSITES PART A-APPLIED SCIENCE AND MANUFACTURING*, 64,
840 159-166.
841 Gurjanov, O. P., Ibragimova, N. N., Gnezdilov, O. I., & Gorshkova, T. A. (2008).
842 Polysaccharides, tightly bound to cellulose in cell wall of flax bast fibre:
843 Isolation and identification. *Carbohydrate Polymers*, 72(4), 719-729.
844 Hayashi, T., Marsden, M. P. F., & Delmer, D. P. (1987). Pea Xyloglucan and Cellulose:
845 VI. Xyloglucan-Cellulose Interactions in Vitro and in Vivo. *Plant physiology*,
846 83(2), 384-389.

847 Herbaut, M., Zoghlami, A., Habrant, A., Falourd, X., Foucat, L., Chabbert, B., & Paes,
848 G. (2018). Multimodal analysis of pretreated biomass species highlights
849 generic markers of lignocellulose recalcitrance. *Biotechnology for Bifuels,* 11.
850 Herbig, C., & Maier, U. (2011). Flax for oil or fibre? Morphometric analysis of flax
851 seeds and new aspects of flax cultivation in Late Neolithic wetland settlements
852 in southwest Germany. *Vegetation History and Archaeobotany,* 20(6), 527-533.
853 Herrera, L. K., Justo, A., Duran, A., de Haro, M. C. J., Franquelo, M., & Rodriguez, J.
854 L. P. (2010). Identification of cellulose fibres belonging to Spanish cultural
855 heritage using synchrotron high resolution X-ray diffraction. *Applied Physics a-*
856 *Materials Science & Processing,* 99(2), 391-398.
857 Himmelsbach, D. S. (2002). Mid-IR imaging of natural fibers. *Abstracts of Papers of the*
858 *American Chemical Society,* 224, U632-U632.
859 Kacurakova, M., Capek, P., Sasinkova, V., Wellner, N., & Ebringerova, A. (2000). FT-
860 IR study of plant cell wall model compounds: pectic polysaccharides and
861 hemicelluloses. *Carbohydrate Polymers,* 43(2), 195-203.
862 Kavkler, K., Gunde-Cimerman, N., Zalar, P., & Demsar, A. (2011). FTIR spectroscopy
863 of biodegraded historical textiles. *Polymer Degradation and Stability,* 96(4), 574-
864 580.
865 Kolodziejski, W., & Klinowski, J. (2002). Kinetics of cross-polarization in solid-state
866 NMR: A guide for chemists. *Chemical Reviews,* 102(3), 613-628.
867 Kvavadze, E., Bar-Yosef, O., Belfer-Cohen, A., Boaretto, E., Jakeli, N., Matskevich, Z.,
868 & Meshveliani, T. (2009). 30,000-year-old wild flax fibers. *Science,* 325(5946),
869 1359-1359.
870 Lahaye, M., Bouin, C., Barbacci, A., Le Gall, S., & Foucat, L. (2018). Water and cell
871 wall contributions to apple mechanical properties. *Food Chemistry,* 268, 386-
872 394.
873 Lahaye, M., Falourd, X., Laillet, B., & Le Gall, S. (2020). Cellulose, pectin and water in
874 cell walls determine apple flesh viscoelastic mechanical properties.
875 *Carbohydrate Polymers,* 232, 10.
876 Larsson, P. T., Wickholm, K., & Iversen, T. (1997). A CP/MAS C-13 NMR
877 investigation of molecular ordering in celluloses. *Carbohydrate Research,* 302(1-
878 2), 19-25.
879 Lazic, B., Janjic, S., Rijavec, T., & Kostic, M. (2017). Effect of chemical treatments on
880 the chemical composition and properties of flax fibers. *Journal of the Serbian*
881 *Chemical Society,* 82(1), 83-97.
882 Le Duigou, A., & Castro, M. (2016). Evaluation of force generation mechanisms in
883 natural, passive hydraulic actuators. *Scientific Reports,* 6, 9.
884 Lefeuvre, A., Baley, C., & Morvan, C. (2018). Analysis of flax fiber cell-wall non-
885 cellulosic polysaccharides under different weather conditions (Marylin
886 variety). *Journal of Natural Fibers,* 15(4), 539-544.
887 Lefeuvre, A., Bourmaud, A., Lebrun, L., Morvan, C., & Baley, C. (2013). A study of
888 the yearly reproducibility of flax fiber tensile properties. *Industrial Crops and*
889 *Products,* 50, 400-407.

Lefeuvre, A., Bourmaud, A., Morvan, C., & Baley, C. (2014). Tensile properties of elementary fibres of flax and glass: Analysis of reproducibility and scattering. *Materials Letters,* 130, 289-291.

Lefeuvre, A., Duigou, A. L., Bourmaud, A., Kervoelen, A., Morvan, C., & Baley, C. (2015). Analysis of the role of the main constitutive polysaccharides in the flax fibre mechanical behaviour. *Industrial Crops and Products,* 76, 1039-1048.

Leroy, A., Falourd, X., Foucat, L., Méchin, V., Guillon, F., & Paës, G. (2021). Evaluating polymers interplay to investigate lignocellulos recalcitrance. *Biotechnology for Bifuels*.

Lindeberg, G. (1948). Tensile strength and chemical composition of the middle lamella of the flax fibre. *Experientia*, 476–477.

McDougall, G. J. (1993). Isolation and partial characterization of the non-cellulosic polysaccharides of flax fiber. *Carbohydrate Research,* 241, 227-236.

Melelli, A., Arnould, O., Beaugrand, J., & Bourmaud, A. (2020). The middle lamella of plant fibers used as composite reinforcement : investigation by Atomic Force Microscopy. *Molecules,* 25(3), 17.

Melelli, A., Shah, D., Hapsari, G., Cortopassi, R., Durand, S., Arnould, O., . . . Bourmaud, A. (2021). Lessons on textile history and fibre durability from a 4000-year-old Egyptian flax yarn. *Nature Plants*.

Mellerowicz, E. J., & Gorshkova, T. A. (2011). Tensional stress generation in gelatinous fibres: a review and possible mechanism based on cell-wall structure and composition. *Journal of Experimental Botany,* 63(2), 551-565.

Mohanty, A. K., Vivekanandhan, S., Pin, J. M., & Misra, M. (2018). Composites from renewable and sustainable resources: Challenges and innovations. *Science,* 362(6414), 536-542.

Morvan, C., Andeme-Onzighi, C., Girault, R., Himmelsbach, D. S., Driouich, A., & Akin, D. E. (2003). Building flax fibres: more than one brick in the walls. *Plant Physiology and Biochemistry,* 41(11-12), 935-944.

Morvan, C., Andème-Onzighi, C., Girault, R., Himmelsbach, D. S., Driouich, A., & Akin, D. E. (2003). Building flax fibres: more than one brick in the walls. *Plant Physiology and Biochemistry,* 41(11), 935-944.

Muller, M., Murphy, B., Burghammer, M., Riekel, C., Roberts, M., Papiz, M., . . . Pantos, E. (2004). Identification of ancient textile fibres from Khirbet Qumran caves using synchrotron radiation microbeam diffraction. *Spectrochimica Acta Part B-Atomic Spectroscopy,* 59(10-11), 1669-1674.

Newman, R. H. (1999). Estimation of the lateral dimensions of cellulose crystallites using C-13 NMR signal strengths. *Solid State Nuclear Magnetic Resonance,* 15(1), 21-29.

Newman, R. H., & Davidson, T. C. (2004). Molecular conformations at the cellulose-water interface. *Cellulose,* 11(1), 23-32.

Nilsson, T., & Gustafsson, P. J. (2007). Influence of dislocations and plasticity on the tensile behaviour of flax and hemp fibres. *Composites Part a-Applied Science and Manufacturing,* 38(7), 1722-1728.

933 Perremans, D., Hendrickx, K., Verpoest, I., & Van Vuure, A. W. (2018). Effect of
934 chemical treatments on the mechanical properties of technical flax fibres with
935 emphasis on stiffness improvement. *Composites Science and Technology,* 160,
936 216-223.
937 Pettolino, F. A., Walsh, C., Fincher, G. B., & Bacic, A. (2012). Determining the
938 polysaccharide composition of plant cell walls. *Nature Protocols,* 7(9), 1590-
939 1607.
940 Pillin, I., Kervoelen, A., Bourmaud, A., Goimard, J., Montrelay, N., & Baley, C. (2011).
941 Could oleaginous flax fibers be used as reinforcement for polymers? *Industrial*
942 *Crops and Products,* 34(3), 1556-1563.
943 Placet, V., Cisse, O., & Boubakar, M. L. (2014). Nonlinear tensile behaviour of
944 elementary hemp fibres. Part I: Investigation of the possible origins using
945 repeated progressive loading with in situ microscopic observations.
946 *COMPOSITES PART A-APPLIED SCIENCE AND MANUFACTURING,* 56,
947 319-327.
948 Ray, S., Vigouroux, J., Quemener, B., Bonnin, E., & Lahaye, M. (2014). Novel and
949 diverse fine structures in LiCl-DMSO extracted apple hemicelluloses.
950 *Carbohydrate Polymers,* 108, 46-57.
951 Richely, E., Bourmaud, A., Placet, V., Guessasma, S., & Beaugrand, J. (2021). A critical
952 review of the ultrastructure, mechanics and modelling of flax fibres and their
953 defects. *Progress in Materials Science*, 100851.
954 Richely, E., Durand, S., Melelli, A., Kao, A., Magueresse, A., Dhakal, H., . . .
955 Guessasma, S. (2021). Novel insight into the intricate shape of flax fibre lumen.
956 *Fibers,* 9(4), 17.
957 Rihouey, C., Paynel, F., Gorshkova, T., & Morvan, C. (2017). Flax fibers : Assessing
958 the non-cellulosic polysaccharides and an approach to supramolecular design
959 of the cell wall. *Cellulose,* 24(5), 1985-2001.
960 Robert, P., Marquis, M., Barron, C., Guillon, F., & Saulnier, L. (2005). FT-IR
961 investigation of cell wall polysaccharides from cereal grains. Arabinoxylan
962 infrared assignment. *J Agric Food Chem,* 53(18), 7014-7018.
963 Romhany, G., Karger-Kocsis, J., & Czigany, T. (2003). Tensile fracture and failure
964 behavior of technical flax fibers. *Journal of Applied Polymer Science,* 90(13), 3638-
965 3645.
966 *Saunders, M., A., K., B., , Maes, C., Akle, S., & Zahr, M. PDCO: Primal-dual interior*
967 *method for convex objectives. Software available at http://www. stanford.*
968 *edu/group/SOL/software/pdco.*(2002).
969 Synytsya, A., Čopíková, J., Matějka, P., & Machovič, V. (2003). Fourier transform
970 Raman and infrared spectroscopy of pectins. *Carbohydrate Polymers,* 54(1), 97-
971 106.
972 Videcoq, P., Barbacci, A., Assor, C., Magnenet, V., Arnould, O., Le Gall, S., & Lahaye,
973 M. (2017). Examining the contribution of cell wall polysaccharides to the
974 mechanical properties of apple parenchyma tissue using exogenous enzymes.
975 *Journal of Experimental Botany,* 68(18), 5137-5146.

976 Weiss, E., & Zohary, D. (2011). The neolithic southwest asian founder crops their
977 biology and archaeobotany. *Current Anthropology,* 52, S237-S254.
978 Zhou, X.-L., Sun, P.-N., Bucheli, P., Huang, T.-H., & Wang, D. (2009). FT-IR
979 Methodology for Quality Control of Arabinogalactan Protein (AGP) Extracted
980 from Green Tea (Camellia sinensis). *Journal of Agricultural and Food Chemistry,*
981 57(12), 5121-5128.
982 Zuckerstatter, G., Terinte, N., Sixta, H., & Schuster, K. C. (2013). Novel insight into
983 cellulose supramolecular structure through C-13 CP-MAS NMR spectroscopy
984 and paramagnetic relaxation enhancement. *Carbohydrate Polymers,* 93(1), 122-
985 128.
986 Zuluaga, R., Putaux, J. L., Cruz, J., Vélez, J., Mondragon, I., & Gañán, P. (2009).
987 Cellulose microfibrils from banana rachis: Effect of alkaline treatments on
988 structural and morphological features. *Carbohydrate Polymers,* 76(1), 51-59.

989

Flax bundles biopolymers sequential extraction

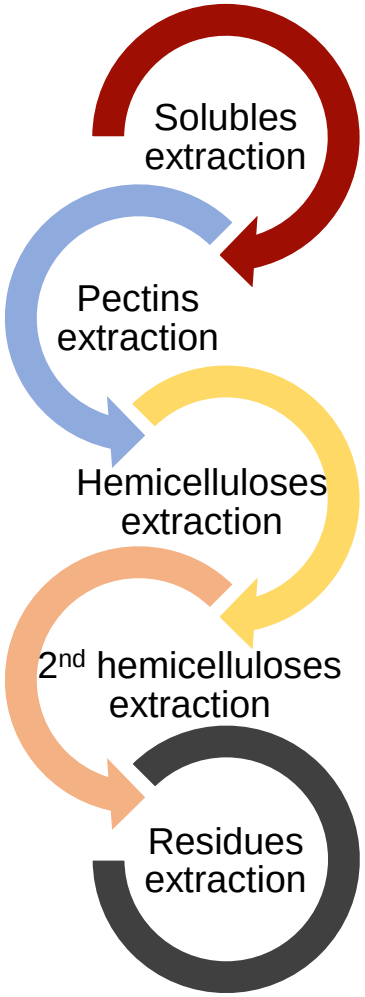

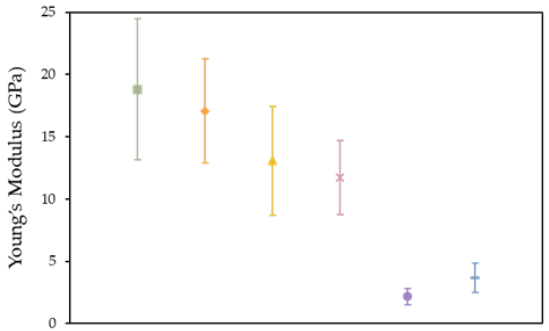

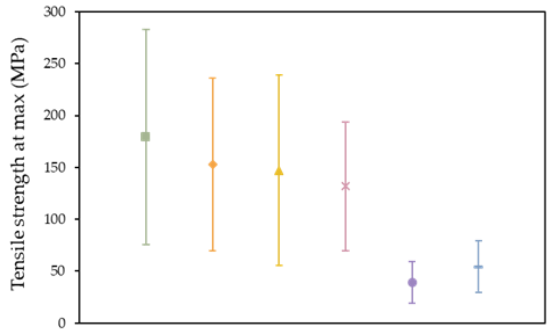

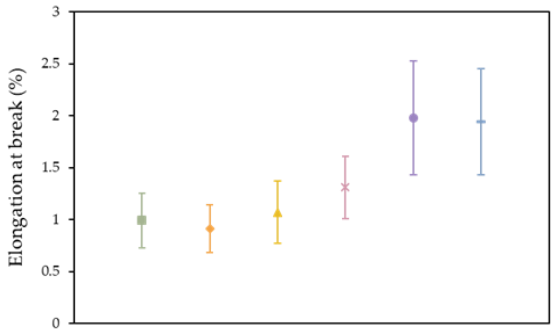

How can we explain the **differences** on **mechanical behaviour** at **fibre bundles** scale ?

Elimination of **middle lamella** + **Individualization**

Successive **extractions** of **monosaccharides**

Cellulose structure **changes**

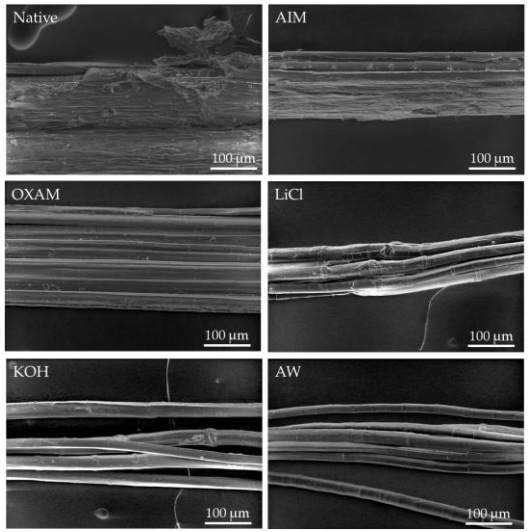

Pectins
HG, RG-I and AG-II

Hemicelluloses
GM and XG

Hemicelluloses + residual pectins
XG and AG-II